

Properties of the electron beam in a room-temperature electron beam ion source investigated by position sensitive x-ray detection

A. Silze,^{1,a)} G. Zschornack,¹ V. P. Ovsyannikov,² and F. Ullmann²

¹*Institut für Angewandte Physik, Technische Universität Dresden, Helmholtzstraße 10, D-01062 Dresden, Germany*

²*DREEBIT GmbH, Zur Wetterwarte 50, D-01109 Dresden, Germany*

(Received 17 April 2008; accepted 29 June 2008; published online 21 August 2008)

The evolution of the charge state distribution inside an electron beam ion source or trap (EBIS/T) is determined by interactions of the electron beam with the ions in the trap region. Hence, detailed information about the electron beam is required for evaluations of spectroscopic and ion extraction measurements performed at EBIS/T facilities. This article presents the results of investigations on the electron beam properties of an ion source of the Dresden EBIS type. For the first time theoretical predictions of the shape of the beam were tested for a noncryogenic EBIS working with low magnetic flux densities provided by permanent magnets. Position and width of the electron beam were measured at different electron energies showing an oscillation in the beam structure. At an energy of $E_e = 16$ keV and an emission current of $I_e = 30$ mA the beam is compressed to a radius of $r_e = 57$ μm (80% current). This refers to an average current density of $\langle j_e \rangle = 232$ A/cm². © 2008 American Institute of Physics. [DOI: 10.1063/1.2960568]

I. INTRODUCTION

Highly charged ions (HCIs) have become an important subject of investigation in many domains of pure as well as applied physics.¹ Spectroscopic investigations on radiation emitted by HCIs allow direct observation of QED effects in their electronic structure^{2,3} and, therefore, are an important tool in modern basic research. Spectra from HCIs give information about radiative and collisional processes in laboratory and astrophysical plasmas.^{4,5} Furthermore, beams of HCIs are used in a variety of fields including surface modification and analysis^{6–8} as well as cancer treatment by ion radiation therapy.⁹

Electron beam ion sources and traps (EBISs/Ts) are capable of producing HCIs at a wide range of elements and ion energies. This flexibility is advantageous, if not essential, for many applications mentioned above. However, the ion currents provided by EBIS/T systems are low in comparison to traditionally applied electron cyclotron resonance or liquid metal ion sources. In order to improve the performance and viability of existing EBIS/T technology a better understanding of the physics of these ion sources is required. In particular, this concerns the properties of the electron beam as well as its interactions with ions in the trap region. The electron beam radius, r_e , and, thus, its current density, j_e , define characteristic ionization times. Accurate values of r_e and j_e , respectively, allow for calculations of cross sections from rates of electron-ion interactions which can be measured in spectroscopic or ion extraction experiments. Electron impact ionization cross sections, for example, play a fundamental role in basic atomic collision physics and are of great interest to plasma modeling.

^{a)}Electronic mail: alexandra.silze@mailbox.tu-dresden.de.

From Herrmann's theory¹⁰ the average radius of the electron beam which includes 80% of the total electron current I_e ¹¹ can be derived as

$$r_h = r_b \sqrt{\frac{1}{2} + \frac{1}{2} \sqrt{1 + 4 \left(\frac{8m_e k T_c r_c^2}{e^2 B_z^2 r_b^4} + \frac{B_c^2 r_c^4}{B_z^2 r_b^4} \right)}}. \quad (1)$$

In this equation

$$r_b = \frac{1}{B_z} \sqrt{\frac{2I_e m_e}{\pi \epsilon_0 v_z e}} \quad (2)$$

is the Brillouin flow radius. The mass and charge of the electron are represented by m_e and e , k is the Boltzmann constant, and r_c is the cathode radius. Temperature and magnetic flux density at the cathode are denoted by T_c and B_c . B_z is the magnetic induction on the beam axis z . The electron velocity in the z direction can be estimated using $v_z = \sqrt{2E_e/m_e}$. Furthermore, theory predicts oscillations of the beam radius with a wavelength of¹²

$$\lambda_h = \frac{4\pi}{\sqrt{\frac{e}{m_e} B_z}} \sqrt{\frac{1}{1 + \frac{B_c^2 r_c^4}{B_z^2 r_b^4}}}, \quad (3)$$

where U given in V corresponds to the electron beam energy E_e in eV.

Previous measurements performed at EBIS/T facilities^{11,13–15} resulted in good agreement between experimental values and average radii r_h predicted by Herrmann's theory. However, the range of parameters in which theoretical calculations had been tested was limited to beam energies above $E_e = 15$ keV and high magnetic flux densities of several teslas provided by superconducting solenoid coils.

The experiments presented in this paper were carried out using an ion source of the Dresden EBIS type.¹⁶ Values of

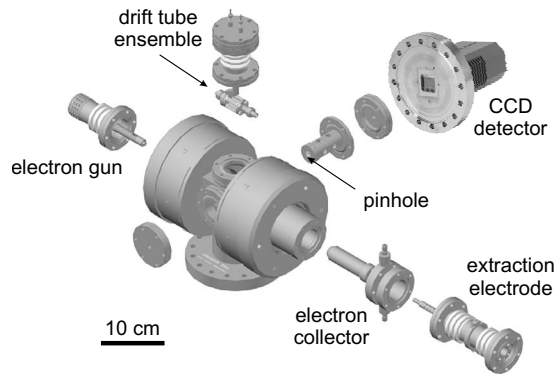


FIG. 1. Setup including the Dresden EBIS and the position sensitive x-ray detection system.

the size of the electron beam were recorded varying the electron energy from $E_e=7$ keV to $E_e=18$ keV and compared to values from theory. One of the prominent features of this source is the application of permanent magnets and additional soft iron components allowing the machine to be operated at room temperature. The nearly constant magnetic flux density in its trap region is an order of magnitude lower compared to other EBIS/T systems. Hence, the new results contribute to the general understanding of the formation of electron beams in EBISs/Ts.

II. EXPERIMENTAL SETUP

The design of the Dresden EBIS^{16,17} is similar to other EBIS/T devices.^{14,18,19} A high-density electron beam emitted by a cathode of $r_c=0.25$ mm operated at $T_c\approx 2000$ K enables electron impact ionization within the source. The negative space charge of the electrons traps the ions in the radial direction. Axial confinement is realized by a box shaped potential created by an ensemble of three collinear drift tube elements. A magnetic field of $B_z=400$ mT on the electron beam axis within the drift tube region compresses the beam to its final diameter and current density.

Interactions between electrons and ions are studied by spectroscopic investigations as well as ion extraction and analysis. Radiation from the ions inside the trap can be detected in perpendicular direction to the electron beam via view ports. Extraction of the ions is realized by switching the potential of a drift tube element that closes or opens the trap in the axial direction. An analysis of the ion beam extracted from the source then provides information about the charge state distribution inside the trap after a certain ionization time.

For the experiments described in this paper additional equipment had been attached to the side flanges of the Dresden EBIS, as sketched in Fig. 1. In order to study the electron beam width and position, a support device was designed to place a pinhole with a diameter of $d=50$ μm close to the drift tube region. The distance of the aperture to the beam axis z was set to 24 mm. In the x' - z' -plane, on the other side of the aperture, a charge coupled device (CCD) detector with an efficiency between 10% and 90% for photons from 1 eV to 10 keV was installed with a distance of 302 mm. The resulting magnification factor was 12.6.

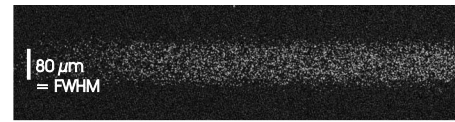


FIG. 2. Two-dimensional x-ray picture of the electron beam.

III. X-RAY IMAGING OF THE ELECTRON BEAM

Figure 2 shows an example for two-dimensional pictures taken with the setup described in Sec. II. The full width half maximum of line scans through the two-dimensional intensity distribution given in Fig. 2 is 67 pixels on the screen referring to an approximate beam width of 80 μm . This gives a first impression of the order of magnitude of the electron beam diameter. However, for further projects such as the determination of cross sections the accuracy of such estimations is not sufficient. Hence, the principle of data acquisition and evaluation had to be improved.

According to Fig. 2, the width of the beam does not change significantly along the detected area which is reasonable considering the ratio of detected beam length and overall trap length of about 1/60. Therefore, the information in the z' dimension could be neglected and the two-dimensional image $I(x', z')$ was turned into a one-dimensional intensity profile $I(x')$ leading to an improvement of the statistics of the measured distribution. The z' axis of the screen was aligned to the beam axis z with the help of the two-dimensional pictures. Afterward, the pinhole was replaced by a slit of $d=50$ μm . During all following experiments, the camera was used in horizontal binning mode meaning the charges accumulated on the CCD were readout in horizontal lines instead of separate pixels. Compared to line scans through the two-dimensional pictures this way of measuring the profile of the beam increased the signal-to-noise ratio by a factor of 3.

In order to improve the accuracy of the method, it also had to be taken into account that the diameter of the slit was in the same order of magnitude as the electron beam width which had to be measured. This problem was solved as illustrated in Fig. 3. Assuming the density distribution of electrons and ions to be Gaussian in the radial direction with equal widths, $\sigma_e=\sigma_i=\sigma$, the intensity profile of the beam along the x axis is determined as

$$I(x) \sim e^{-x^2/2\sigma_e^2} e^{-x^2/2\sigma_i^2} = e^{-x^2/\sigma^2}. \quad (4)$$

The part of the intensity $I(x)$ from a specific point x which is emitted under an appropriate solid angle passes the slit before it is spread evenly over a respective region $D(x)$ on the

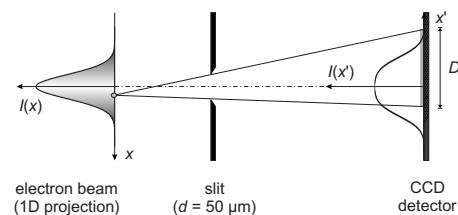


FIG. 3. Principle of electron beam imaging by position sensitive x-ray detection.

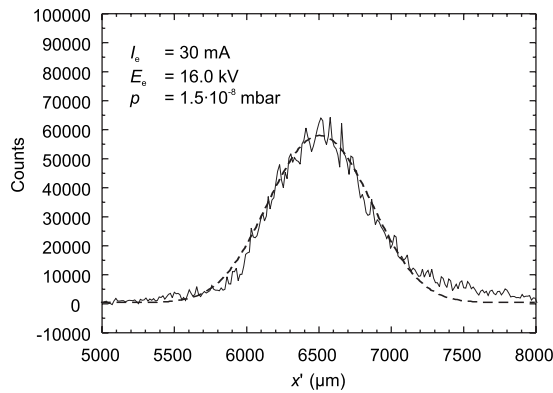


FIG. 4. Solid line: intensity distribution on the CCD detector. Dashed line: fit according to Eq. (5).

detector, as shown in the scheme in Fig. 3. The distance between the electron beam and the slit is much larger than the electron beam diameter. Therefore, the solid angle for the radiation reaching the detector and the width D of the illuminated area can be considered to be uniform for every x . Only the boundaries of $D(x)$ on the x' axis change when x is varied. An integration over all points x from which radiation is emitted delivers the resulting intensity distribution $I(x')$ on the camera

$$I(x') \sim \operatorname{erf}\left(\frac{1}{\sigma\mu}\left[x' + (1 + \mu)\frac{d}{2}\right]\right) - \operatorname{erf}\left(\frac{1}{\sigma\mu}\left[x' - (1 + \mu)\frac{d}{2}\right]\right), \quad (5)$$

where $\mu=12.6$ denotes the ratio between object distance and image distance.

However, Eq. (5) can only be applied to evaluate measured intensity profiles if the width of the ion distribution does not widely exceed the electron beam width. Therefore, we kept the temperature of the ions low by setting the axial trap potential to zero. Test measurements of energy dispersive x-ray spectra had shown that the signal created by HCIs inside the source would still be sufficient. This assures that hot ions leave the trap in the axial direction instead of moving away from the electron beam region in the radial direction. The electron energy during the measurements was set to $E_e=16$ keV and the electron beam current was $I_e=30$ mA. The pressure inside the source was kept at $p=1.5 \times 10^{-8}$ mbar using xenon as the injected gas. Under these experimental conditions the standard derivation of the Gaussian beam profile resulting from a fit of Eq. (5) to the measured intensity distribution is $\sigma=(32 \pm 5)$ μm . This refers to a radius which contains 80% of the two-dimensional Gaussian beam distribution of $r_e=(57 \pm 9)$ μm and a mean current density of $\langle j_e \rangle=(232 \pm 72)$ A/cm². The errors of these values correspond to a limited accuracy of the slit diameter d and the magnification factor μ . The conformity of the fitted and measured data can be seen in Fig. 4.

IV. VARIATION OF THE ELECTRON BEAM ENERGY

As presented in Sec. I, Herrmann's theory predicts an oscillation of the electron beam width along the z axis. Due

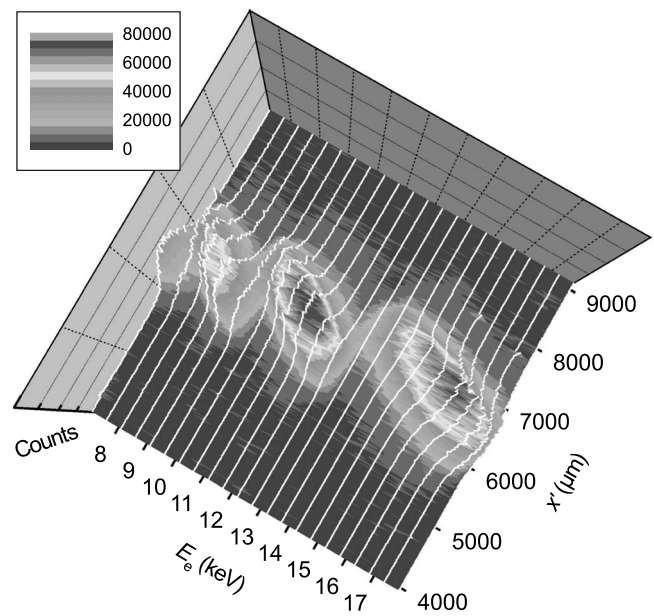


FIG. 5. The intensity distribution on the CCD screen at different electron energies, E_e , indicating the structure of the electron beam along the z axis. White lines: curves measured according to Fig. 3.

to several experimental conditions, we could not observe this effect directly. The section of the electron beam imaged on the screen was too small compared to the overall beam length and the position of the detected beam area could not be changed along the z axis. Still, it was necessary to gain information about the electron beam diameter on a larger scale to exclude the possibility of having measured the width at a particularly wide or narrow part of the electron beam which does not represent the average value.

To circumvent this problem, we changed the wavelength of the oscillation instead of the position of the detector. This can be achieved by a variation of the electron beam energy as given by Eq. (3). It relates the wavelength of the oscillation λ_h to the electron beam energy E_e in the following way:

$$\lambda(E_e) \sim \sqrt{E_e}. \quad (6)$$

Thus, if the cathode and the imaging system positions are fixed and the electron beam energy E_e is varied maxima and minima of the beam oscillations will alternately pass the detector position. Therefore, it is possible to scan the electron beam properties along the z axis.

Figure 5 shows the corresponding experimental result. The intensity profile at the detector is shown in relation to the applied electron beam energy. In fact, a periodical change in the profile of the intensity distribution on the detector was measured. However, instead of an oscillating diameter, a periodical shift in the position of the beam as well as an alternating signal intensity was observed. This allows interpretations of an electron beam following spiral trajectories which conflict with the traditional assumption of a rotationally symmetric beam geometry. Such effects appear if the surface normal of the cathode is not parallel to the lines of magnetic flux of the source. The alternating intensity arises due to a periodically varying angle between the small imaged section of the spiral-like beam and the direction of the slit. Lowering the electron energy stepwise from $E_e=17.75$ keV to E_e

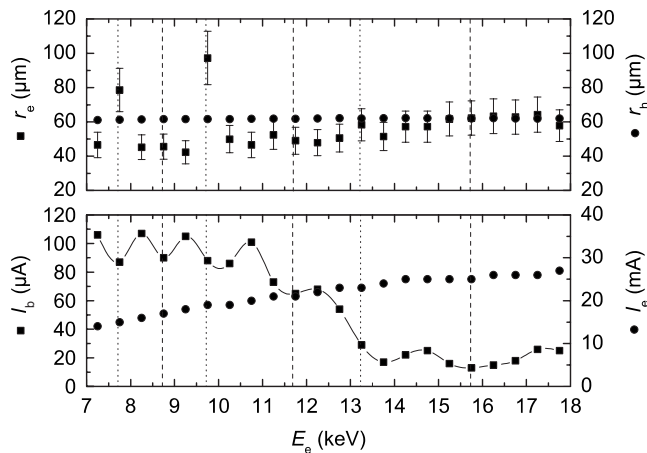


FIG. 6. Top: measured electron beam radii, r_e , (squares) and the calculated Herrmann radii, r_h , (circles) under variation of the electron beam energy, E_e . Bottom: reactive current, I_b , (squares) and total electron current, I_e , (circles) during the variation of the electron beam energy, E_e . Dashed and dotted vertical lines indicate the maxima and minima of the intensity on the screen, respectively (see Fig. 5).

$=7.25$ keV, the intensity reaches a maximum at the same energy which had been applied when the detector axis z' was aligned to the beam. Two more maxima were recorded during the electron energy variation. In between, minima appear when the directions of the imaged part of the beam and the slit differ the most.

Intensity maxima on the detector are achieved at $E_{e,n}=15.8$ keV, $E_{e,n+1}=11.6$ keV, and $E_{e,n+2}=9.0$ keV, as shown in Fig. 5. The index n denotes the number of maxima within the distance $l=51.7$ mm between the cathode and the detected beam area. With the n th maximum being situated at the center of the imaged beam section, l is a multiple of the wavelength of the oscillation λ_n . This relation can be written as

$$l = n\lambda_n \sim n\sqrt{E_{e,n}}, \quad (7)$$

from which the respective number of maxima along the distance l can be calculated with

$$n = \frac{\sqrt{E_{e,n+1}}}{\sqrt{E_{e,n}} - \sqrt{E_{e,n+1}}}. \quad (8)$$

The experimental values for $E_{e,n}$, $E_{e,n+1}$, and $E_{e,n+2}$ correspond to the sixth, seventh, and eighth maxima which are visible on the screen. These maxima are related to the wavelengths $\lambda(9.0 \text{ keV}) \approx 6.5$ mm, $\lambda(11.6 \text{ keV}) \approx 7.4$ mm, and $\lambda(15.8 \text{ keV}) \approx 8.6$ mm which show that the wavelength of the beam periodicity is indeed proportional to the square root of the electron energy.

To study the relation between the measured profile and the energy of the electron beam in detail, line cuts of the three-dimensional plot in Fig. 5 at certain energies were evaluated as presented in Sec. III. The electron radii, r_e , and corresponding theoretical average values calculated according to Herrmann's theory, r_h , are shown in the upper part of Fig. 6. In general, calculation and measurement are in good agreement, especially for energies above $E_e=13$ keV. In the lower energy range, specifically at $E_e=7750$ eV and $E_e=9750$ eV, aberrations from theory appear which coincide

with intensity minima due to unfavorable angles of slit and beam direction and, thus, have to be neglected. Theory also overestimates the beam radii at lower electron energies by 20%.

The source parameters I_e and I_b during the experiment can be seen in the lower part of Fig. 6. The electron loss current on the drift tubes, I_b , oscillates with half the wavelength of the position shift. The total electron current, I_e , continuously decreases as the electron energy drops. In combination with the measured beam radii this information indicates that the electron current density does not vary significantly along the spiral propagation of the beam.

Calculations assuming ideal conditions predict oscillating electron beam radii with amplitudes which would exceed the measurement error. The insufficiency of the theoretical description of the shape of the electron beam mainly appears because of two simplifications. The electron velocity in the longitudinal direction is considered to be uniform. Thermal effects on the longitudinal velocity distribution of the electrons lead to chromatic aberrations in Herrmann's optical theory of the electron beam which reduces the detectable amplitude of the variation of the beam radius. Furthermore, the trajectories of the electrons are disturbed by imperfections of the rotational symmetry of the source. This causes additional beam variations which diminish the effect of the initial oscillation.

V. SUMMARY AND PROSPECTS

Electron beam radii and current densities of the Dresden EBIS were measured for various electron energies and currents. The results of this investigation expand the range of parameters in which Herrmann's theory has been tested to room-temperature EBISs working with low magnetic fields. In contrast to theoretical predictions these experiments did not show a significant oscillation of the electron current density but a periodic shift in the beam position along the electron-optical axis of the source. Nevertheless, average beam radii are in good agreement with Herrmann's theory. This conclusion is of high interest for experimental investigations dealing with interactions of the electron beam with the ions in the trap region of EBIS/T systems.

Recent projects at Dresden EBIS/T facilities involve the determination of electron impact ionization cross sections from the evolution of the charge state distribution inside the source. Numbers of ions of a specific charge state extracted from the source have been recorded at various ionization times in the range of $t_{\text{trap}}=1$ ms to several seconds. Electron current densities measured as described in this paper can be used to derive the cross sections from this data. In order to improve the precision of this method the diameter of the ion cloud and, thus, the overlap ratio between electron beam and ion distribution additionally have to be measured. Preparations of a corresponding investigation including optical imaging of the trap region are currently in progress.

ACKNOWLEDGMENTS

We thank René Heller, Ulrich Kentsch, Martin Kreller, and Mike Schmidt for assistance during the experiments.

This work was supported by the EFRE fund of the EU and by the Freistaat Sachsen (Project Nos. 12321/2000 and 12184/2000).

- ¹J. D. Gillaspay, *J. Phys. B* **34**, R93 (2001).
- ²P. Beiersdorfer, H. Chen, D. B. Thorn, and E. Träbert, *Phys. Rev. Lett.* **95**, 233003 (2005).
- ³H. Bruhns, J. Braun, K. Kubicek, J. R. Crespo López-Urrutia, and J. Ullrich, *Phys. Rev. Lett.* **99**, 113001 (2007).
- ⁴P. Beiersdorfer, R. E. Olson, G. V. Brown, H. Chen, C. L. Harris, P. A. Neill, L. Schweikhard, S. B. Utter, and K. Widmann, *Phys. Rev. Lett.* **85**, 5090 (2000).
- ⁵P. Beiersdorfer, K. R. Boyce, G. V. Brown, H. Chen, S. M. Kahn, R. L. Kelley, M. May, R. E. Olson, F. S. Porter, C. K. Stahle, and W. A. Tilloston, *Science* **300**, 1558 (2003).
- ⁶G. Hayderer, S. Cernusca, M. Schmid, P. Varga, H. P. Winter, F. Aumayr, D. Niemann, V. Hoffmann, N. Stolterfoht, C. Lemell, L. Wirtz, and J. Burgdörfer, *Phys. Rev. Lett.* **86**, 3530 (2001).
- ⁷T. Schenkel, A. Persaud, A. Kraemer, J. W. McDonald, J. P. Holder, A. V. Hamza, and D. H. Schneider, *Rev. Sci. Instrum.* **73**, 663 (2002).
- ⁸F. Ullmann, F. Grossmann, V. P. Ovsyannikov, J. Gierak, and G. Zschornack, *Appl. Phys. Lett.* **90**, 083112 (2007).
- ⁹D. Schulz-Ertner, A. Nikoghosyan, C. Thilman, T. Haberer, O. Jäkel, C. Karger, G. Kraft, M. Wannenmacher, and J. Debus, *Int. J. Radiat. Oncol., Biol., Phys.* **58**, 631 (2004).
- ¹⁰G. Herrmann, *J. Appl. Phys.* **29**, 127 (1958).
- ¹¹H. Kuramoto, T. Kinugawa, H. Watanabe, C. Yamada, S. Ohtani, I. Yamada, and F. J. Currell, *Rev. Sci. Instrum.* **73**, 42 (2002).
- ¹²I. V. Alyamovsky, *Electron Beams and Electron Guns* (Sovetskoe Radio, Moscow, 1966), p. 417.
- ¹³M. A. Levine, J. N. Marrs, J. N. Bardsley, P. Beiersdorfer, C. L. Bennett, M. H. Chen, T. Cowan, D. Dietrich, J. R. Henderson, D. A. Knapp, A. Osterheld, B. M. Penetrante, M. B. Schneider, and J. H. Schofield, *Nucl. Instrum. Methods Phys. Res. B* **43**, 431 (1989).
- ¹⁴D. A. Knapp, R. E. Marrs, S. R. Elliot, E. W. Magee, and R. Zasadzinski, *Nucl. Instrum. Methods Phys. Res. A* **334**, 305 (1993).
- ¹⁵S. B. Utter, P. Beiersdorfer, J. R. Crespo López-Urrutia, and K. Widmann, *Nucl. Instrum. Methods Phys. Res. A* **428**, 276 (1999).
- ¹⁶G. Zschornack, S. Landgraf, F. Grossmann, U. Kentsch, V. P. Ovsyannikov, M. Schmidt, and F. Ullmann, *Nucl. Instrum. Methods Phys. Res. B* **235**, 514 (2005).
- ¹⁷See <http://www.dreebit.com> for further information.
- ¹⁸F. J. Currell, J. Asada, K. Ishii, A. Minoh, K. Motohashi, N. Nakamura, K. Nishizawa, S. Ohtani, K. Okazaki, M. Sakurai, H. Shiraishi, S. Tsurubuchi, and H. Watanabe, *J. Phys. Soc. Jpn.* **65**, 3186 (1996).
- ¹⁹J. R. Crespo López-Urrutia, B. Bapat, I. Draganic, A. Werdich, and J. Ullrich, *Phys. Scr.*, T **92**, 110 (2001).